EFGs on Surfaces – Experiment and Theory

Bengt Lindgren

Department of Physics, University of Uppsala, Box 530, S-75121 UPPSALA, Sweden

Reprint requests to Dr. B. L.; E-mail: Bengt.Lindgren@fysik.uu.se

Experimental and calculated electric field gradients (EFG) on various probe atoms at different sites on metal surfaces, are reviewed. The calculations are based on the discrete variational method (DVM) molecular/cluster approach within the local density approximation and the experimental data are mostly obtained with the time differential perturbed angular correlation (TDPAC) method. Recent observations of an increasing EFG with temperature for adsorbed Se on (111) metal surfaces are explained as due to an outward probe relaxation, resulting in an increased EFG. This means that positive EFGs at (111) sites increase whereas negative EFGs at (001) surfaces reduce in magnitude. Previously unpublished results for various Cd-probe sites at Pd(110) are also discussed in detail.

Key words: Electric Field Gradient; Surface.

1. Introduction

During the last two decades, metal surfaces have been the platform for basic studies of a number of new physical phenomena. Different atomic sites with different symmetry properties are found at substitutional terrace sites, various kink and step sites as well as for adatom positions. Differently shaped atomic agglomerates, e. g. monoatomic chains, can be manufactured on anisotropic surfaces. The electric field gradient (EFG) at nuclear probe atoms is here an excellent "finger print" quantity due to the short ranged dependence on the local charge distribution. The anisotropy factor η directly reflects the deviation from 3- or 4-fold rotational symmetry, and the magnitude and the sign of the EFG strongly depends on the probe distance to the surface layer.

The NMR (nuclear magnetic resonance) and PAC (time differential perturbed angular correlations – TDPAC) techniques have been used in a wide range of applications due to the possibility of using isolated probe atoms ($< 10^{11}$ atoms/cm^2), and several review articles have described the experimental status [1 - 5]. In particular, the sensitive ^{111}In/^{111}Cd-PAC probe nucleus has been used by the Konstanz group [1 - 4] for surface studies and experimental EFGs for a number of different sites and surfaces have been determined.

In Sect. 3 some of their results will be compared to theoretical values.

For ionic systems, the EFG is often deduced from point charge calculations. The method has also been used for metallic systems, then based on a parameterisation into one part, V_{zz}(ext), originating from sources external to the electronic shell of the probe atom, and another part, V_{zz}(el), from the valence electrons or unfilled atomic orbitals local to the probe nucleus:

$$V_{zz} = (1 - \gamma_{\infty})V_{zz}(\text{ext}) + (1 - R)V_{zz}(\text{el}). \qquad (1)$$

The polarization of the charge distribution in the core is accounted for by the Sternheimer antishielding factors γ_{∞} and R. The first term is often calculated by a lattice summation of point charges. Relying on the so called "universal correlation", discovered by Raghavan *et al.* [6] the second term can be estimated to be three times the first term but with opposite sign. However, with increasing amount of available data and, in particular, determinations of the sign of the EFG, this proportionality has been questioned in many systems [7]. The systematic oscillatory dependence of the EFG as function of probe atom in one and the same host, e. g. hcp Cd-metal, is but one example. In the beginning of the 5sp-series (Ag-Sn) the EFG is positive, while it is negative at the end of the series. This
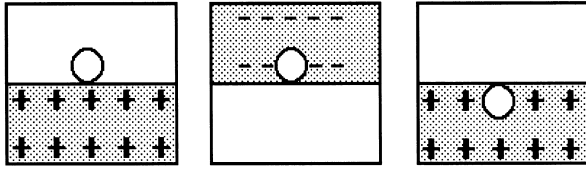
Fig. 1. Schematic picture of the adatom site (left) which is equivalent to a cubic bulk structure (zero EFG) with the upper half of the host charges removed (center) or with the complementary charge system shown in the right figure. Hence, only a sign change is expected compared to the EFG of a substitutional site (right).

is caused by a population differences of the $5p_x$, p_y and $5p_z$ orbitals [8], not accounted for by antishielding factors. Another example is found by comparing the EFG at substitutional terrace and adatom sites on a surface. As will be shown in Sect. 3, these EFGs differ by an order of magnitude but, if only equivalent charges or potentials external to the probe atom are considered, the two sites are complementary (Fig. 1) and only a change in the sign of the EFG is expected.

Determinations of population as well as polarization differences of the valence orbitals require the evaluation of electronic wave functions, often best determined by band-structure calculations, see e. g. [9 - 11]. However, most of the measured EFGs are for impurity probe atoms. The broken symmetry then requires large super cells in order to exclude impurity-impurity interactions. Another approach, which makes use of the short range dependence of the EFG, is the molecular-cluster method, where self-consistent solutions are found for the electronic wave functions in a cluster of a limited number of atoms. A detailed description is given in Sect. 2 and the suitability of the method for obtaining the EFG at various sites on surfaces is discussed in Sect. 3. In general, the magnitude of the EFG decreases with increasing temperature, as $T^{-3/2}$ in bulk systems and as T^{-1} on surfaces, but recently an increase with temperature of the EFG at Se adatoms on (111) surfaces was found [12]. This will be discussed in Section 4. Finally a summary is given.

2. Method

2.1. Computational Procedure

The theoretical basis for the electronic-structure calculations in the discrete variational method (DVM)

code [13] is the self-consistent one-electron local density formalism in the spin unrestricted Hartree-Fock-Slater model [14]. The essential point of this theory is the replacement of the nonlocal Hartree-Fock exchange operator by a potential depending only on the local electron density: "local density approximation - LDA".

In a non relativistic approach the one-electron Hamiltonian for the molecule can be written (in Hartree atomic units au) as

$$H = -\frac{1}{2}\nabla^2 + V_\mathrm{C} + V_\mathrm{xc}, \qquad (2)$$

where the first two terms are the kinetic energy and Coulomb potential. The Hedin-Lundqvist [15] and the Barth-Hedin potential [16] were adopted for the exchange-correlation potential V_xc.

As in the usual linear-combination-of-atomic-orbital-molecular-orbital (LCAO-MO) method, the molecular-orbital eigenfunctions are expanded in terms of symmetry orbitals:

$$\Psi_i(\boldsymbol{r}') = \sum_j \chi_j(\boldsymbol{r}') \cdot C_{ji}. \qquad (3)$$

The symmetry orbitals χ_j are chosen here as linear combinations of atomic orbitals located on the different atoms in the molecule corresponding to the cluster point group symmetry, i. e.,

$$\chi_j(\boldsymbol{r}') = \sum_{\nu,n,l,m} W_{\nu m}^{jl} \cdot U_{nl}(r_\nu) \cdot \mathrm{Y}_{lm}(\hat{r}_\nu), \quad (4)$$

where $U_{nl}(r_\nu)$ is the atomic radial wave function centered on the νth nucleus, with principal quantum number n and orbital number l. U_{nl} is obtained numerically by solving a self-consistent free atom or ion problem, and Y_{lm} is a spherical harmonic function with magnetic quantum number m. $W_{\nu m}^{jl}$ are symmetrization coefficients which can be obtained by group-theoretical projection operators. In this work a double basis, composed of neutral and ionized atoms was used for the probe atom for which the EFG was determined. This kind of basis has enough variational freedom to reproduce all major rearrangements in the valence electron density [17]. For certain systems, a less accurate single basis set had to be used for the other host atoms due to technical limitations in the program. Core orbitals were "frozen", i. e. the cores were only present in the overlap matrix but not in the
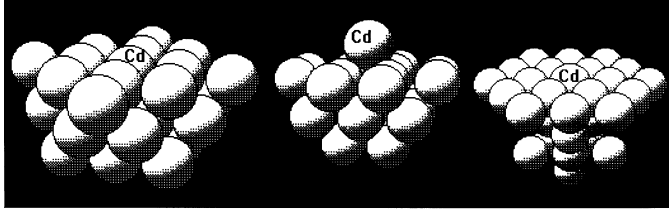
Hamiltonian matrix. Relaxing the core for the probe atom did not change the result of the EFG calculation.

The expansion coefficients (variational coefficients) C_{ji} are obtained using standard procedures by solving the matrix secular equation

$$(\boldsymbol{H} - \varepsilon\boldsymbol{S})\boldsymbol{C} = 0, \tag{5}$$

where ε is the eigenvalue matrix. The Hamiltonian matrix $\boldsymbol{H}$ and the symmetry orbital overlap matrix $\boldsymbol{S}$ are obtained in the discrete variational method [13] as a weighted sum over a set of sample points. A pseudo random Diophantine distribution [18] is mapped onto an infinite domain representing the region exterior to atomic spheres of some arbitrary radius, using a Fermi distribution, and in the core regions near the nucleus, an optimised Gaussian surface mesh is used in conjunction with a radial Simpson's rule scheme in spheres centered on the nuclei.

The Fermi energy and the occupation numbers $f_i(\varepsilon)$ for each molecular orbital (MO) in (3) are obtained by applying Fermi-Dirac statistics on these MO eigenstates. The cluster charge density is then constructed by summing over all MO's:

$$\rho_{\text{cluster}}(\boldsymbol{r'}) = \sum f_i \cdot |\Psi_i(\boldsymbol{r'})|^2 . \tag{6}$$

In order to calculate the potential by one-dimensional integration, this charge density is cast in a multicenter-overlapping multipolar form [17]

$$\rho_{\text{model}}(\boldsymbol{r'}) = \sum_{njlm} d_{jlm}(n) \cdot \rho_j(r_n) \cdot Y_{lm}(\hat{r}_n), \tag{7}$$

where $r_n = r - R_n$, R_n are atomic sites, and (j, l, m) denotes multipoles centered on various nuclear sites. The coefficients $\{d_{jlm}\}$ are determined by least-squares fitting to the eigenvector density in (6). The radial density basis set of $\{\rho_j\}$ was constructed from wave function variational basis, and from spherical radial functions for each $l \leq 2$ in the fully symmetric representation of the molecular point group. In the

self-consistent multipolar (SCM) procedure the potential calculated from this representation of the cluster density is used to determine new wave functions and hence a new cluster density, until self-consistency is obtained.

Different cluster geometries representing different surfaces are shown in Figure 2. All interatomic distances were representative for the bulk metal. An optimisation of the geometry with minimisation of the total energy is not possible with the present numerical integration accuracy.

2.2. Cluster Embedding

When representing a solid by a finite cluster of atoms, it is necessary to consider the embedding problem. For treating some properties of metals which may depend more or less sensitively on the band structure, it is desirable to broaden the discrete energy levels of the isolated cluster into bands. This can be accomplished by empirical level-smearing schemes – a technique often used to draw smooth density of state curves from the discrete energy levels, or by modifying the cluster boundary conditions. The asymptotic form of the wave function can be controlled by mixing in a selected continuum state into the cluster wave functions and solving the inhomogeneous Schrödinger equation [19]. The net result is an energy-dependent broadening of cluster levels and a smooth spectral representation of properties like the charge and spin densities. In this work an empirical level smearing was used. Each energy level was broadened by

$$L_i(E) = (\beta/4) \cosh^{-2}[\beta(E - \varepsilon_i)/2]. \tag{8}$$

The actual population for each single-particle state is obtained by integrating up to the Fermi energy ε_{F}, i. e. by the well-known Fermi distribution function

$$f_i = \int_{-\infty}^{\varepsilon_{\text{F}}} L_i(E)\,\mathrm{d}\,E = \{1 + \exp[\beta(\varepsilon_i - \varepsilon_{\text{F}})]\}^{-1}. \tag{9}$$
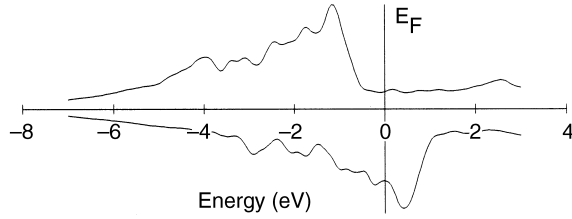
Fig. 3. Density of states as obtained from a $CdCo_{54}$ "bulk-like" cluster.

The choice of the smearing function is arbitrary. Fine details in the density of states (DOS) are not significant, since it is only the total occupation of each state that is controlled self-consistently through (6). However, the broadening parameter β depended on the amount of the 3d-character of each state, since 3d-bands are narrower than sp-valence bands. For the 3d contributions to the energy states $\beta = 300$ (au.) was chosen, while for the sp contributions $\beta = 50$ was used. Hence, the pure Ni and Co 3d-energy levels were 6 times sharper than the sp-states, ensuring a good determination of the magnetic moments while keeping the accuracy of the hyperfine field and electric field gradient (EFG). These mainly originate from Cd s- and p-states, respectively. Figure 3 shows the DOS from a $CdCo_{54}$ cluster approximating bulk Co-metal. In a few cases, the more time consuming but parameter-free plane-wave matching of the cluster wave functions [19] was also used, but without any significant change of the results.

2.3. Electric Field Gradient and Hyperfine Field

From the obtained wave functions, the self-consistent charge density $\rho(\boldsymbol{r})$ was calculated as well as all components of the EFG tensor (given in atomic units):

$$V_{ij} = - \int \rho(\boldsymbol{r'})\frac{3r_i r_j - \delta_{ij}r^2}{r^5}\, d\boldsymbol{r'} + V_{ij}(\text{nuclear}). \quad (10)$$

The second term $V_{ij}(\text{nuclear})$ is a summation of the nuclear or ionic point-like charges with the same geometric weight factor as in the first term. The conversion factor between atomic and SI units is $9.72 \cdot 10^{21}$ V/m²au. Here V_{ij} refers to the cluster coordinate system. The dominant contribution to the total EFG is found to originate from the p-character of the valence orbitals [8, 9], and the core states are mainly

contributing through the orthogonalization requirement to the valence states. When the point group has a three- or fourfold symmetry axis (z), the p_x and p_y orbitals are degenerate and the EFG (V_{zz}) is axially symmetric along this axis. For twofold symmetry, e. g. a (110) surface, an asymmetry factor is defined by $\eta = (V_{xx} - V_{yy})/V_{zz}$, with the principle axis chosen such that $|V_{zz}| \geq |V_{yy}| \geq |V_{xx}|$. For still lower point group symmetries, e. g. step sites, the coordinate system of the cluster does not necessarily correspond to the EFG principal-axis system and a diagonalization of the full EFG tensor must be performed. The EFG is related to the measured quadrupole coupling constant ν_Q and the nuclear quadrupole moment Q_N by

$$\nu_Q = eQ_N V_{zz}/h. \quad (11)$$

The Fermi contact hyperfine field (B_{hf}) may also be calculated (non-relativistically) from the spin density at the probe nucleus by

$$B_{hf} = \left[\rho_{\text{majority}}(0) - \rho_{\text{minority}}(0)\right] \cdot 52.42 \,\text{Tesla}/a_0^3. \quad (12)$$

For magnetic probe atoms, the core contribution to the local magnetic field is rather significant. The core orbitals may then be recalculated in a procedure similar to the initial calculation of a spin polarised free atom. This procedure is not fully self-consistent since the new spin polarised core orbitals may affect the valence orbitals. The hyperfine field can then be separated into a core and a valence term.

3. Surface EFGs

3.1. Cd on (001)-surfaces

The Cu surfaces have been studied extensively after the pioneering work on Cu(001) by the Konstanz
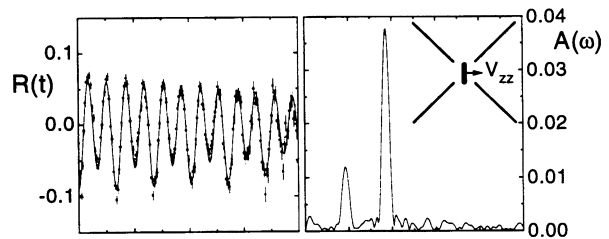

Fig. 4. TDPAC time spectrum for ^{111}Cd on Cu(001) and its fourier transform (data by the author). The detector geometry is shown in the inset. The quadrupole frequency corresponds to $V_{zz} = 9.0 \cdot 10^{21}$ V/m² (using $Q = 0.83$ b).
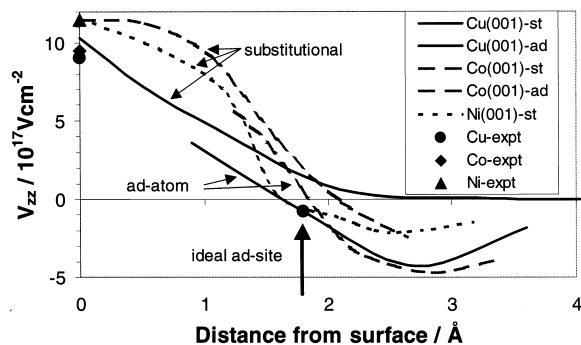
Fig. 5. The EFG calculated on Cd at different distances from the (001) surface layer of fcc Cu, Co and Ni along lines passing through the substitutional terrace and hollow adatom sites respectively. The position of the ideal adatom site (lattice site in the next empty layer above the surface) is indicated. Experimental values [2, 22, 23] are shown with symbols. However, the sign of the EFG can not be determined with PAC.

group [20]. The PAC-data (see Fig. 4) show the frequencies for a well defined, axially symmetric EFG perpendicular to the surface as expected from symmetry. Using a $CdCu_{21}$ cluster, the corresponding EFG was calculated [21] as a function of the probe distance to the surface (see Fig. 5).

The experimental value for the substitutional terrace site on Cu(001) is slightly lower than the calculated one. However, low-energy ion scattering (LEIS) studies on In atoms on a stepped Cu(100) surface [24] show that the In atom in the terrace has a position slightly above (about 0.4 Å) the Cu surface monolayer. Indium is the parent atom which decays to Cd, for which the EFG is measured. It was not possible to determine the geometry by minimisation of the total energy in the calculations, but the calculated and experimental values are in excellent agreement if a 0.4 Å outward relaxation of Cd is allowed (Fig. 5). Also, by plotting charge densities (Fig. 6), it is clear that the bigger Cd-atom would like to relax from the ideal surface lattice site. A qualitative explanation for the distance dependence is also obtained from Figure 6. At 4 Å above the surface, the Cd-atom charge density is essentially spherical, and only a very small EFG is

expected. As the Cd atom approaches the vacant site in the surface layer, a lobe develops towards the surface creating a small negative EFG-contribution. This explains the negative EFGs calculated for adatom sites in Figure 5. Closer to the surface layer the charge in the plane dominates and the EFG becomes positive. In Sect. 4, the consequences of such a change of sign will be discussed in relation to the temperature dependence of the EFG of adsorbed Se atoms on (001) and (111) surfaces.

When the calculations were performed [25], the experimental value of the adatom site was not known, but in later experiments, using low temperature deposition of In/Cd, the site was observed with an EFG in excellent agreement with the calculated value [2]. As already mentioned in the introduction, the two terrace and adsorbed sites are complementary if only equivalent charges and potentials external to the Cd atom are considered (Fig. 1), and only a change in the sign of the EFG would be expected. Clearly the difference must be found in the electron charge distribution local to the Cd probe atom and in particular in the 5p-character of the valence electrons which contribute most significantly to the EFG. The large positive EFG at the substitutional site may either be due to a population difference, with more Cd $5p_x$ and $5p_y$ orbitals in the plane than $5p_z$ perpendicular to the plane, or to a polarization of these orbitals, i.e. they have a different radial extensions. In the previous work [2] we showed that it is a polarization effect which accounts for most of the final EFG. Both the $5p_z$ and the $5p_x$, $5p_y$ charge distributions are contracted compared to a free neutral Cd atom, as expected since 5p is an excited state in the free atom. For the adatom site, the $5p_z$ is slightly more contracted than the $5p_x$, $5p_y$ due to the interaction with the charge from the host atoms in the plane below. However, this difference is small since the nearest neighbouring host atoms are not lying in the direction of the p-lobe, which is the case for the $5p_x$, $5p_y$ lobes at the terrace site. Hence the 5p charge distribution in the plane is much more shifted towards the Cd nucleus with a large positive EFG as a result.
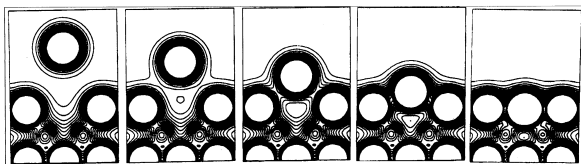

Fig. 6. Charge densities for different Cd distances (4.2, 3.2, 2.1, 1.1 and 0 Å) to the Cu(100) surface layer. Contour level intervals are 0.002 au.
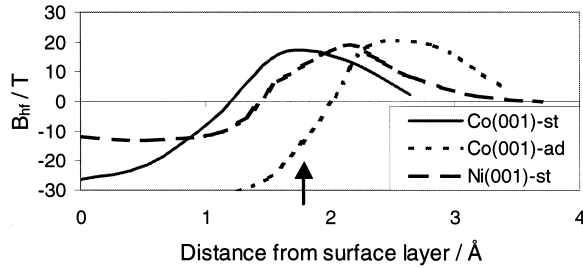
Fig. 7. The variation of the Cd hyperfine field (B_{hf}) with the distance to Ni and Co (001) surfaces, from the substitutional (-st) and through the adatom (-ad) sites. The arrow indicates the ideal adatom site in the next empty layer. For adatom sites at Ni only the ideal adatom site was calculated (B_{hf} = –5.8 T).

Co(100) and Ni(100) behave much the same with a difference to Cu that relates to the lattice constant. For Co and Ni the hyperfine field was also determined [26, 27] (see Fig. 7). Experimental values are only reported for the Ni surfaces [22]: 3.9 T at the substitutional site and 7.2 T at the adatom site. The sign has not been determined. At the moment there is no explanation to this significant difference.

3.2. Cd on (111)-surfaces

By studying the annealing behaviour of the Cd-EFG at Cu(111), the Konstanz group [2] was able to identify several different sites. Their model suggests that the In-parent atom first occupies an adatoms site at low temperatures after the deposition, but very soon diffuses to a step where it first is trapped at an adatom step site. At about 140 K the probe atom is found in a substitutional step site, probably by trapping in a step vacancy, and above 200 K the In atom diffuses into the topmost monolayer in order to occupy the substitutional terrace sites. Similar studies have also been performed for Cu(001) by the same group and more recently by the Groningen group [28] using the soft-landing ion deposition technique on a vicinal cut Cu(17,1,1).

The Cu(111) results for the substitutional and adatom sites resemble those of Cu(001). The substitutional terrace EFG was calculated as V_{zz} = +11.3·10^{21} V/m^2 [21] in agreement with the experimental value of 10.1·10^{21} V/m^2 [2]. The larger value compared to Cu(001) is explained by the denser packing of atoms. The calculated EFG for the ideal adatom site is V_{zz} = –6.2·10^{21} V/m^2 with a distance depen-
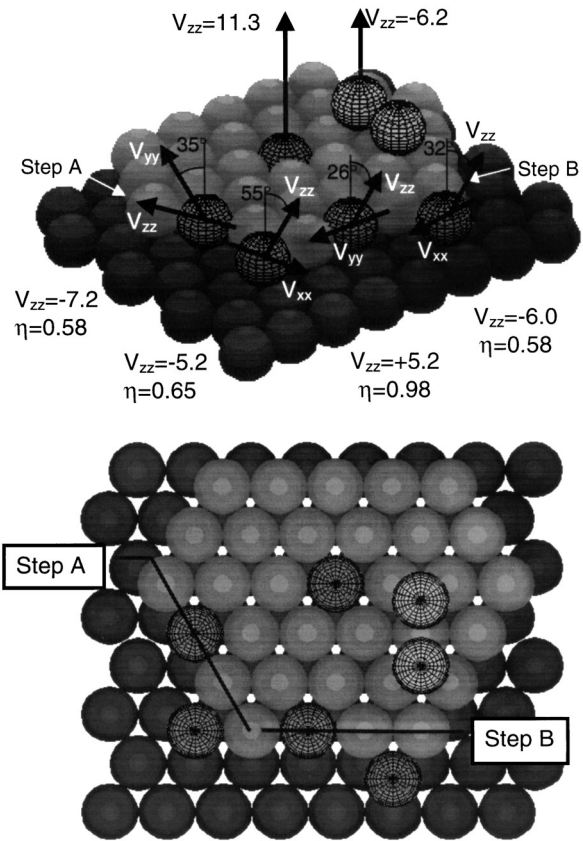

Fig. 8. Calculated EFG (in 10^{21} V/m^2) for Cd at various sites on a Cu(111) surface. The step sites A have C_{2V} symmetry if only the nearest neighbour host atoms are included while sites at step B only have a mirrow symmetry (C_h). Values from [21].

dence similar to Cu(001). No experimental value is reported.

In order to calculate the EFGs for the various step sites on Cu(111) (see Fig. 8) much smaller clusters were used, only including the nearest neighbouring Cu atoms. Partly this was enforced by the lower point symmetry at these sites. The substitutional terrace site then corresponds to a CdCu$_9$ cluster, which gave V_{zz} = 7.8·10^{21} V/m^2 which is somewhat smaller than V_{zz} = 11.3·10^{21} V/m^2 obtained with the CdCu$_{38}$ cluster. Comparing these values, it is evident that most of the EFG is determined by the short ranged interactions of the probe atom with the nearest neighbouring atoms.

Two different types of steps are present on the (111) surface. One of them has the point symmetry C_{2v}
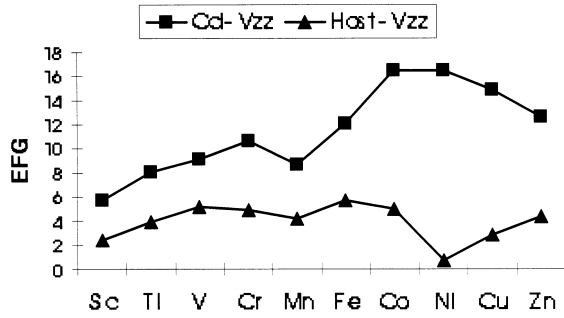
Fig. 9. The EFG (V_{zz} in 10^{21} V/m^2) at different close packed transition metals surfaces.

for both the substitutional and adatom sites at the step if only the nearest Cu atoms are considered. The principle-axis system is here defined by the twofold symmetry axis, 35° to the surface normal. The second step configuration has only a mirror plane symmetry and cross terms between p_x and p_y are present. The orientation of V_{zz}, V_{yy} and V_{xx} is obtained by a diagonalization of the EFG-tensor. The calculated results are summarized in Figure 8.

Experimentally only the EFGs of B type steps are observed. This was verified by measurements on Cu crystals cut along the (667) and (545) surfaces [2]. The adatom step site has $|V_{zz}|$ = 5.8·10^{21} V/m^2, η = 0.37 with V_{zz} at 31° to [1 1 1] and V_{xx} parallel with the step. Our value for η (see Fig. 8) is higher, but otherwise the agreement is very good. Also the values for the substitutional step site agree with the experimental values: $|V_{zz}|$ = 7.8·10^{21} V/m^2, η = 0.69 with V_{zz} at 18° to [1 1 1] and V_{yy} parallel with the step. In particular, the direction of the smallest EFG component distinguishes between the two sites.

3.3. EFGs on Closed Packed 3d-metal Surfaces

The EFGs and magnetic hyperfine fields (B_{hf}) were also calculated for the closed packed 3d-transition metal surfaces [27], both at the host probe atom and at Cd-probes. Due to the unfrozen 3d-orbitals only a single 3d4s4p host basis set was used which seemed to overestimate the magnitude of both the EFG and B_{hf} compared to systems where a double host basis could be used. The result is summarized in Table 1 and Figure 9.

Except for a small dip at Mn, the EFG on Cd increases slightly with the number of d-electrons as expected from the corresponding reduction in the interatomic distance. Figure 9 also show the EFG at the

Table 1. The EFG (10^{21} V/m^2), the 3d magnetic moment, $\mu_d(\mu_B)$ and valence contribution to the hyperfine field, B_{hf} (Tesla) at the substitutional terrace site at different close-packed 3d-transition metal surfaces.

Surface	Host-probe				Cd-probe		
	V_{zz}	η	μ_d	$B_{hf,val}$	V_{zz}	η	B_{hf}
Sc-hcp(0001)	+2.4				+5.7		
Ti-hcp(0001)	+3.9				+8.1		
V-bcc(110)	+5.2	0.2			+9.1	0.2	
Cr-bcc(110)	+4.9	0.1	2.6	+32.7	+10.7	0.1	–27.3
Mn-fcc(111)	+4.2		3.4	+8.6	+8.7		–57.1
Fe-bcc(110)	+5.7	0.1	2.6	+7.6	+12.1	0.1	–35.6
Co-fcc(111)	+5.0		1.7	0.0	+16.5		–30.9
Co-hcp(0001)	+5.0		1.7	+0.9	+15.6		–24.3
Ni-fcc(111)	+0.7		0.7	+0.7	+16.5		–13.0
Cu-fcc(111)	+2.9				+11.3		
Zn-hcp(0001)	+4.4				+12.6		

host surface atom, without Cd-atoms in the cluster. Blaha et al. [9] have shown that also for bulk hcp 3d-metals the main contribution to the EFG originates from the local valence p-type orbitals. This seems also to be true for the surface host atoms since no systematic variation with the number of d-electrons is observed for their EFG, although the low value for Ni may perhaps be associated with the almost full d-shell.

For the Cd probe, only hyperfine fields at Ni surfaces are reported [22]. The calculated hyperfine field of Cd at Ni(111) is much larger than the experimental value of –6.7(1) T, although previous calculations [26] with a more extended Ni basis showed a better agreement, –7.3 T. Ni magnetism is difficult to treat accurately within the molecular/cluster method due to the small exchange energy, but also the exact Cd position must be known. If the Cd atom is pushed up from the surface, as is known to be the case on Cu(100) [24], the value becomes less negative, and at about 2 Å above the surface it is even positive (+13 T), similar to what was obtained for Cd on Ni(100) (Fig. 7).

Mössbauer measurements (CEMS) have been performed on iron surfaces by Korecki and Gradmann [29]. They were able to resolve the hyperfine interaction contributions from the first (surface) and second monolayers of ^{57}Fe on free Fe(110) surfaces and obtained a quadrupole interaction of –0.18(4) mm/s corresponding to an EFG of V_{zz} = +4.3·10^{21} V/m^2 (using Q = 0.16·10^{-28} m^2, β = 90° and assuming $\eta \approx 0$). This is in reasonable agreement with the calculated EFG, +5.7·10^{21} V/m^2. We have also compared with full potential LMTO calculations [30] of

the Fe(001) surface which should only have a somewhat smaller EFG. Using the expansion of the charge density within the Muffin-tin sphere by Hjortstam et al we obtained an EFG of $+1.1 \ 10^{21}$ V/m^2, while the contribution from external Muffin-tin spheres is only $-0.1 \ 10^{21} V/m^2$. We did not include the charge distribution in the interstitial region but do not expect any large contribution from that. The low value may be due to the less dense (001) surface compared to (110), although the corresponding difference for the EFG on Cd on Cu(001) and Cu(111) is not so pronounced.

Although this paper focuses on the EFG, a short discussion of the magnetic hyperfine field on Fe is appropriate since a reduced hyperfine field is measured at the surface despite an enhanced magnetic moment [29]. The contact hyperfine field originates from the local s-electrons. For the host atoms, with their own 3d-moment, the core s-orbitals are exchange polarized, i.e. the radial shapes of the two spin orbitals are different. This core polarization contribution was calculated separately as described in Sect. 2.3. It is usually negative, scaling with the local magnetic moment. The valence contribution to B_{hf} originates partly from a population difference due to the more abundant majority valence s-states, and partly from a polarization effect. The obtained moments (Table 1) follow the general prediction that as the atom moves towards the surface, the magnetic moment increases towards the free atom value. Nevertheless, we calculated a reduction of the magnitude of B_{hf} of 1.6 T, from –27.0 T, obtained with a "bulk-like" cluster with the probe Fe in the center, to –25.4 T with Fe in the surface layer. The experimental values are –33.0 T and –30.9 T, respectively [29], a difference of 2.1 T. Lower values, in particular of the core exchange contribution, are often obtained in non-relativistic calculations. Taking the ratio, the agreement is much better, 0.94 both experimentally and from the calculations. Ohnishi et al. [31], using FLAPW, also found that the hyperfine field is less negative due to a more positive valence contribution on a Fe(100) surface than in the bulk, but their scalar relativistic hyperfine fields in bulk Fe are closer to the experimental values than our non-relativistic results.

3.4. Cd on (110)-surfaces and Nanostructured Systems

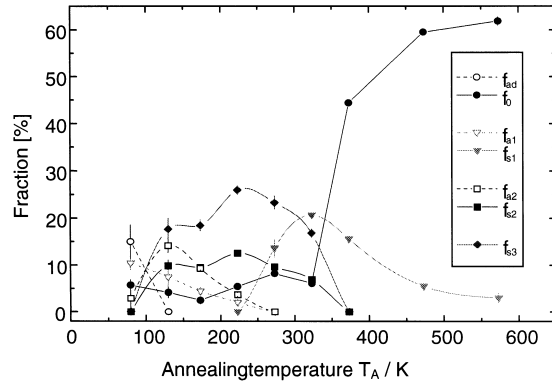The anisotropic (110) surface of fcc metals has a pronounced row structure where one-dimensional

Fig. 10. ^{111}In/^{111}Cd probe fractions as functions of different annealing temperature (from [32]).
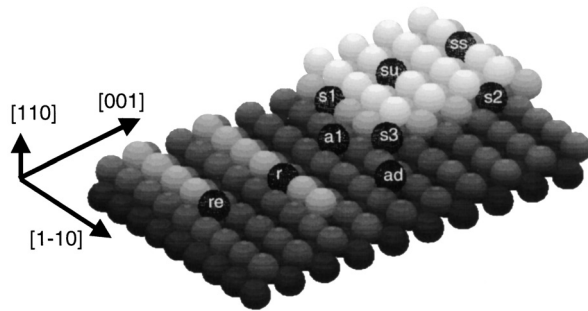

Fig. 11. Different sites of adsorbates on a (110) surface.

systems such as monoatomic chains of e. g. magnetic materials may be grown. At low coverage the evaporated atoms arrange themselves along the <110> rows in the plane with some average length but with the distance between the rows being large enough to neglect inter-row interactions. TDPAC experiments on ^{111}In/^{111}Cd on Pd(110) were initiated by the Konstanz group [32] in order to learn more about adsorption sites and surface diffusion of In adsorbates on such surfaces. ^{111}In was deposited on Pd(110) at 80 K and PAC time spectra were recorded during isochronical annealing (see Fig. 10). Molecular / cluster calculations were also carried out by the present author in order to give support to the site identification of the various frequency fractions observed in the isochronical annealing experiments. The 9 different sites, which were considered, are shown in Figure 11.

Figure 12 shows the cluster geometry used for the Cd-probe in a substitutional (110) terrace site ("su" in Fig. 11). The calculations (Table 2) show that the main EFG-component (V_{zz}) lies along the closed-

Table 2. Calculated EFGs for different sites at a Pd(110) surface. [1 1 0] is the surface normal, [1 $\bar{1}$ 0] the direction of the closed-packed row in the surface plane and [0 0 1] the direction in the plane perpendicular to that row. Site identifications in the first column refers to Figure 11. Also included are the assigned experimental values from the Konstanz group [32]. The value for the row end site (re) is actually for an adsorbed site outside a [0 0 1] step. The sign of the EFG is not possible to determine with PAC.

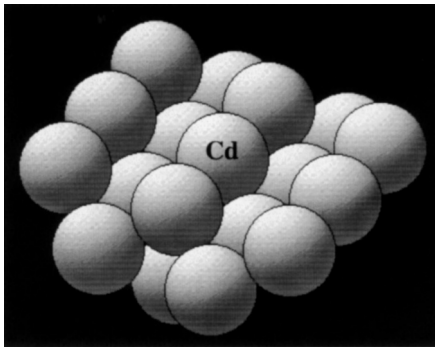| Site	V_{zz} 10^{21} V/m²	η	Orientation, [1 1 0] = surface normal (Fig. 11)
su (110) terrace	−7.2	0.97	V_{zz} [1 $\bar{1}$ 0], V_{yy} [1 1 0]
lexptl:	7.9(12)	0.97(2)	V_{zz} [1 1 0], V_{yy} [1 $\bar{1}$ 0]
r [1 $\bar{1}$ 0] row	+7.7	0.93	V_{zz} [1 1 0]
ss in [1 $\bar{1}$ 0] step	+7.1	0.95	V_{zz} 2° to [1 1 0]
ad (110) adatom	−8.3	0.28	V_{zz} [001], V_{yy} [1 1 0]
lexptl:	8.5(13)	0.42(3)	V_{zz} [1 1 0]
a1 ad-step [1 $\bar{1}$ 0]	−8.2	0.23	V_{zz} [0 0 1] – 1°, V_{yy} [1 1 0]
lexptl:	10.1(15)	0.36(3)	V_{zz} [1 1 0] – 10(3)°, V_{yy} [1 $\bar{1}$ 0]
re [1 $\bar{1}$ 0] row end	+7.7	0.10	V_{zz} 19° to [1 1 0], V_{yy} [0 0 1]
lexptl:	8.0(12)	0.11(4)	V_{zz} 29(3) to [1 1 0], V_{yy} [0 0 1]
s1 (11$\bar{1}$) facett	+9.1	0.07	V_{zz} 35° to [1 1 0] (⊥ facett)
lexptl:	10.2(15)	0.13(5)	V_{zz} 29(3)° to [1 1 0]
s2 (100) facett	+9.1	0.12	V_{zz} 49° to [1 1 0] (∼⊥ facett)
lexptl:	6.1(9)	0.16(2)	V_{zz} 9(2)° to [1 1 0]
s3 step corner	+8.7	0.94	V_{zz} 34° to [1 1 0]
lexptl:	10.2(15)	0.71(4)	V_{zz} 74(4)° to [1 1 0]
Cu (110) terrace	+10.3	0.72	V_{zz} [1 $\bar{1}$ 0], V_{yy} [1 1 0]
lexptl: [33]	7.9(12)	0.74(1)	V_{zz} [1 1 0], V_{yy} [1 $\bar{1}$ 0]
Cu (110) adatom	+8.9	0.62	V_{zz} [0 0 1], V_{yy} [1 $\bar{1}$ 0]
lexptl:	–	–	
Ag (110) terrace	+7.2	0.75	V_{zz} [1 $\bar{1}$ 0], V_{yy} [1 1 0]
lexptl: [33]	7.0(11)	0.80(1)	V_{zz} [1 1 0], V_{yy} [1 $\bar{1}$ 0]
Ag (110) adatom	+7.1	0.60	V_{zz} [0 0 1], V_{yy} [1 $\bar{1}$ 0]
lexptl:	–	–	

Fig. 12. CdPd$_{19}$ cluster with Cd in a Pd(110) terrace position.

packed Pd [1 1 0] row in disagreement with the experimental result, although the perpendicular component is almost as large with an asymmetry factor η close to 1. A relaxation of the surface layer towards the bulk makes the perpendicular component larger. However, if the Cd atom is relaxed out of the plane, the in plane component increases, and hence V_{zz}, at
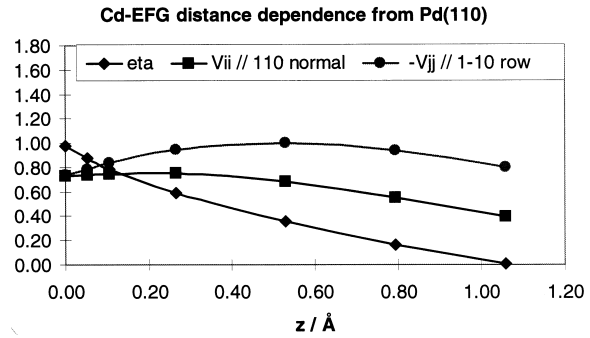

Fig. 13. EFG (10^{21} V/m²) as a function of Cd distance from the surface layer. The dominant inplane component increase as Cd is relaxed out from the surface and η reduce.

least up to a 0.5 Å relaxation (see Fig. 13). This is contrary to what is obtained for more close packed surfaces such as Cu(100) or Ni(100) where an outward relaxation of the oversized Cd/In probe also is observed experimentally [24]. If the two neighbour host atoms in the same [1 $\bar{1}$ 0] row as the Cd atom are relaxed, we expect a smaller in plane contribution and a V_{zz} along the surface normal, but this has not been verified.

The contribution to the EFG from the two rows on both sides of the close-packed row with the Cd-atom, is quite small. Removing both of them (row site "r" in Fig. 11) makes the perpendicular component slightly larger than the magnitude of the in-plane component, while the magnitudes of V_{zz} and η remain almost the same. A similar result is obtained if one of the rows is removed, which corresponds to a substitutional step site ("ss" in Fig. 11). Consequently we do not expect any difference between the calculated EFG at a row end ("re") and for Cd adsorbed at or in a [0 0 1] step (corresponding to "s2" but without the top layer).

The short range dependence of the EFG is also observed for the adatom site ("ad" in Fig. 11), where all the 8 surface Pd-atoms are removed compared to the cluster shown in Figure 12. This value is very similar to what is obtained for In/Cd trapped at an ad-site at a [1 $\bar{1}$ 0] step ("a1" in Fig. 11). The magnitude of the ad-site EFG is similar to the substitutional site, in contrast to the Cu(100) surface where they differed by an order of magnitude. However, the distance between the planes is much smaller for the (110) surface structure. Figure 14 shows the electron density in a (1$\bar{1}$0) plane, perpendicular to the surface and the closed packed rows.
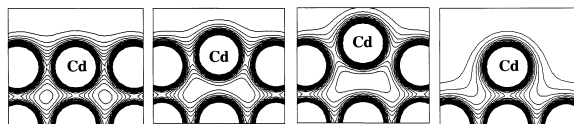
Fig. 14. Electron densities in a plane perpendicular to the Pd(011) surface and [1 1 0] rows. From left to right: Cd substitutional, 0.5 Å, 1.0 Å above the surface and at an adatom site. The Pd atoms in the next layer below Cd (surface layer for the rightmost figure) are not seen in this cut. Contour levels are plotted between 0 and 0.1 au in steps of 0.005 au.

The largest EFG is expected for {111} facet sites ("s1") with values comparable to (111) surfaces, but with a different orientation relative the surface normal.

Table 2 also shows the experimental values obtained and assigned to the various sites by the Konstanz group [32]. It should be mentioned that the determination of the full orientation of the EFG is a great challenge for the experimentalists, in particular when several fractions of different sites are present. Different detector geometries relative to the surface have to be used, as well as a simultaneous fit of all TD-PAC time spectra using non-analytical theory functions [34]. If measurements on magnetic monoatomic chains are to be carried out, a full knowledge of all EFGs is crucial in order to analyse the time-spectra of the combined interaction.

The Konstanz group [32] also studied agglomeration of Cu atoms on a Pd(110) surface with 4% of a monolayer Cu deposited at 223 K before the PAC-isotope ^{111}In was deposited at the same temperature. We do not expect any significant difference between the EFG-contribution from Cu compared to Pd. New calculations for the Cu(110) and Ag(110) surfaces are also included in Table 2 for comparison. In particular the sites in an isolated Cu row ("r" in Fig. 11), at an end of a row ("re") and at an (11$\bar{1}$) facet ("s1") could be identified. By comparing the ratio of the fractions, row lengths between 7 and 9 atoms were deduced, assuming equal occupation probability.

4. Temperature Dependence of the EFG at Se Adatoms

Usually the magnitude of the EFG decreases with increasing temperature, due to increased lattice vibrations and thermal expansion. In non cubic bulk metals, a $T^{-3/2}$ behaviour often describes the temperature dependence, whereas on surfaces a T^{-1} dependence
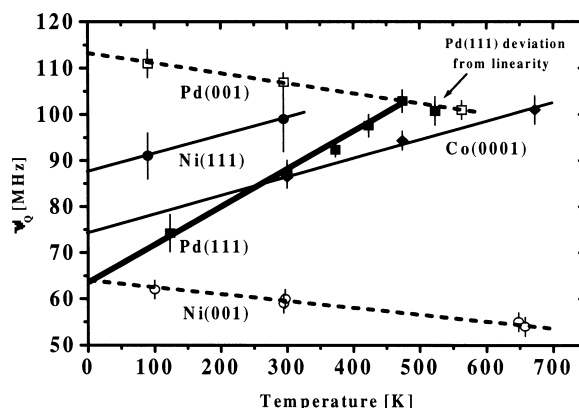

Fig. 15. Temperature dependence of the quadrupole coupling constant ν_Q of ^{77}Se on various surfaces. The relation between ν_Q and V_{zz} is given by (11) with $Q_N = 0.76$ b. However, the sign is not determined.

is usually observed. In general, the observation of the temperature variation of the EFG at adatoms is hampered by the fact that already at lower temperatures adatoms are mobile and may move to traps like steps and kinks. Chalcogens are an exception, and here ^{77}Br/^{77}Se offers a suitable PAC-isotope which has been used by the Berlin group in collaboration with ISOLDE [35]. On Ni(001) and Pd(001) surfaces the precursor Br (and the probe Se) occupies the fourfold hollow adatom site, and at Ni(111), Pd(111) and Co(0001) surfaces the threefold hollow site. At Pd(001) and Ni(001) the expected linear decrease of the EFG was observed but, surprisingly enough, the magnitude of the EFG increased with temperature on the closed packed (111) and (0001) surfaces [12] (see Fig. 15).

As the temperature increases we may expect an increase of the distance of the Se probe atoms from the surface. The previous electron structure calculations on Cd at Cu surfaces (Sect. 3.1, Fig. 5) showed a distance dependence of the EFG with a negative slope and that the adatom site was close to a zero crossing. For a positive V_{zz}, as at substitutional sites, this implies that the magnitude of the EFG is reduced, but for a negative V_{zz} an increase of the magnitude is expected. To test this idea we performed a number of calculations for Se adatoms at various surfaces [12].

The calculated distance dependence of the EFG at Se is shown in Figure 16. The first observation is that the slope is opposite compared to the EFG at Cd. Close to the surface, V_{zz} is negative, and further away it becomes positive. At a substitutional Pd(111)
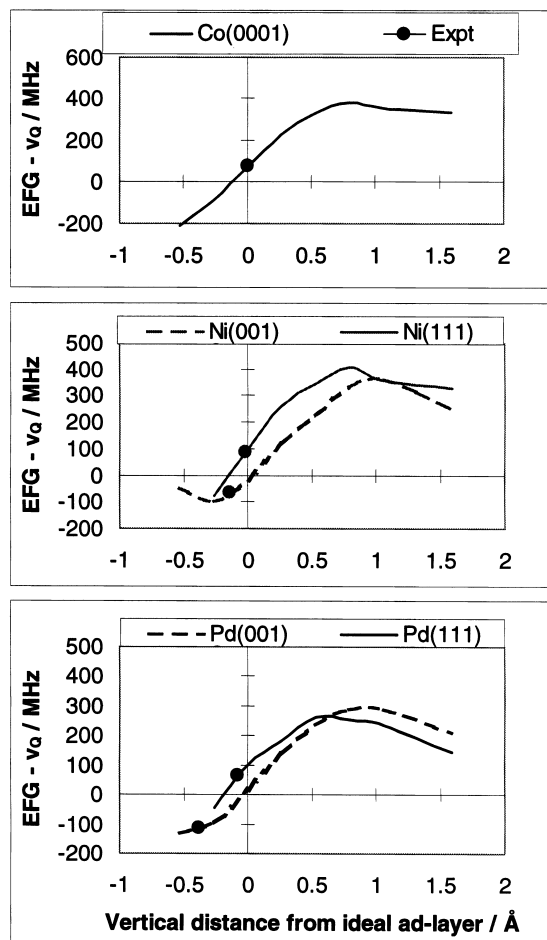
Fig. 16. Calculations of the EFG of ^{77}Se, converted to ν_Q (Q_N = 0.73 b), as a function of the probe distance to the ideal adatom site in the next empty layer above the surface layer. The experimental values (symbols) have been inserted at the distance which agrees with the calculated curves.

terrace site a value of $-14.3 \cdot 10^{21}$ V/m^2 is obtained, corresponding to a quadrupole frequency of $\nu_Q = -263$ MHz. The reason for the opposite sign, compared to Cd, lies in the more than half full 4p-shell of Se. The explanation is analogous to that of the systematic EFG dependence for 5sp-probes in Cadmium metal [8]. With an sp-probe atom at a substitutional site in the surface layer, the splitting of the valence p_x, p_y-orbitals (or bands) into bonding and antibonding states is larger than for the p_z orbitals, due to the lack of neighbours out of the plane (see Fig. 17). For atoms with a less than half filled p-shell this implies a higher occupation of p_x, p_y than of p_z, and hence a positive
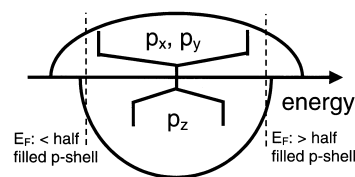

Fig. 17. Schematic illustration of the splitting of the valence p-states into bonding and antibonding states, when the atom is at a substitutional site in the surface layer.

EFG (as for Cd although the free atom has no 5p). For atoms with more than 3 valence p-electrons the population of p_z is dominant and the EFG is negative (as for Se). For sites well above the surface, the situation is the opposite since the splitting of the p_z-states is larger due to the interaction with the surface, while the p_x, p_y have no neighbours.

Experimental values have been inserted in Fig. 16 at distances that give a consistent picture of the temperature dependence. The (001) sites have a negative EFG, which reduces in magnitude when the atoms are relaxed outwards from the surface with temperature. At fcc (111) and hcp (0001) the EFG is positive and becomes more positive with relaxation. Other observations give further justification to the distance assignment. (i) Impurity adatoms at (001) are expected to be closer to the surface than at (111) surfaces due to the larger interplane distance. (ii) Because of the smaller lattice parameter in Ni the adatom is more distant to the Ni surface as compared to Pd. (iii) Photoelectron diffraction experiments [36] on one Se monolayer adsorbed on Ni(111) and Ni(001) were also interpreted in terms of a shorter distance between the Se layer and the surface compared to the ideal adlayer distance (–0.23 Å and –0.21 Å resp). However, it should be pointed out that the calculations are "0 K" calculations, and conclusions about the temperature dependence are only based on changes in interatomic distances.

5. Summary

Examples of hyperfine interactions, and in particular electric field gradients on surfaces have shown the fruitful combination of ultra high vacuum technology, nuclear quadrupole interaction experiments, such as PAC and "computer experiments" such as the DVM-LDA molecular/cluster method. All essential features of the EFG and the hyperfine field of Cd and Se probe atoms at various transition metal surfaces are

well reproduced by first-principle molecular / cluster calculations, using reasonably large clusters. In particular, the calculations give support in determining the probe site, which is not always known directly from the experiments.

Although a conservative estimate of the calculated EFG accuracy is about $1 - 2 \cdot 10^{21} \mathrm{V/m^2}$, or even worse if too restricted basis sets are used, these errors are often systematic, related to the reduction of the bulk metal to a limited number of atoms in a cluster. Hence, systematic variations of the EFG with e. g. distance or probe-Z are much more reliable. Accurate values of the EFG are of course crucial if nuclear quadrupole moments are to be determined, but equally important is the understanding of what is causing the EFG and why it behaves with temperature or relaxation as it does. With this information at hand, other solid state phenomena, such as surface diffusion, surface / interface magnetism etc. can be successfully studied through the hyperfine interactions - and so it has been done!

[1] G. Schatz, R. Fink, T. Klas, G. Krausch, R. Plazer, J. Voigt, and R. Wesche, Hyperfine Interact. **49**, 395 (1989).

[2] T. Klas, R. Fink, G. Krausch, R. Platzer, J. Voigt, R. Wesche, and G. Schatz, Surf. Sci. **216**, 270 (1989).

[3] G. Schatz, X.L.Ding, R. Fink, G. Krausch, B. Luckscheiter, R. Plazer, J. Voigt, U. Wöhrmann, and R. Wesche, Hyperfine Interact. **60**, 975 (1990).

[4] G. Krausch, R. Fink, K. Jacobs, U. Kohl, J. Lohmüller, B. Luckscheiter, R. Platzer, B.-U. Runge, U. Wöhrmann, and G. Schatz, Hyperfine Interact. **78**, 261 (1993).

[5] D. Fick, Applied Phys. **A 49**, 343 (1989).

[6] P. Raghavan, E. N. Kaufman, R. S. Raghavan, E. J. Ansaldo, and R. A. Naumann, Phys.Rev. B **13**, 2835 (1976).

[7] R. Vianden, Hyperfine Interact. **15/16**, 189 (1983); Hyperfine Interact. **35**, 1079 (1987).

[8] B. Lindgren, Phys. Rev. B **34**, 648 (1986).

[9] P. Blaha, K. Schwartz, and P. Dederichs, Phys.Rev. B **37**, 2792 (1988).

[10] H. M. Petrilli, P. E. Blöchl, P. Blaha, and K. Schwarz, Phys. Rev. B **57**, 14690 (1998).

[11] H. Haas and H. M. Petrilli, Phys. Rev. B **61**, 13588 (2000); H. Haas, Hyperfine Interact. **129**, 493 (2000).

[12] A. Weber, K. Potzer, H. Granzer, H. H. Bertschat, W.-D. Zeitz, M. Dietrich, and B. Lindgren, Phys. Rev. B **64**, 081404(R) (2001).

[13] D. E. Ellis and G. S. Painter, Phys. Rev. B **34**, 648 (1986); D.E . Ellis and D. Guenzburger, Adv. in Quantum Chem. **34**, 51 (1999).

[14] J. C. Slater, The Self-Consistent Field for Molecules and Solids, McGraw-Hill, New York 1974.

[15] L. Hedin and B. I. Lundqvist, J.Phys. C **4**, 2064 (1971).

[16] U. von Barth and L. Hedin, J. Phys. C **5**, 1629 (1972).

[17] B. Delley and D. E. Ellis, J. Chem. Phys. **76**, 1949 (1982).

[18] D. E. Ellis, Int. J. Quantum. Chem. **2S**, 35 (1968).

[19] B. Lindgren and D. E. Ellis, Phys. Rev. B**26**, 636 (1982).

[20] T. Klas, J. Voigt, W. Keppner, R. Wesche, and G. Schatz, Phys. Rev. Lett. **57**, 1068 (1986)

[21] B. Lindgren, Europhys. Lett. **11**, 555 (1990).

[22] J. Voigt, R. Fink, G. Krausch, B. Luckscheiter, R. Platzer, U. Wöhrmann, X. L. Ding, and G. Schatz, Phys. Rev. Lett. **64**, 2202 (1990); J. Voigt, thesis, Konstanz, Germany 1990.

[23] R. Fink, B. Lindgren, Pan Min, and M. Semple, Surf. Sci. **355**, 47 (1996).

[24] M. Breeman, G. Dorenbos, and D. O. Boerma, Nucl. Instrum. Meth. **B64**, 64 (1992).

[25] B. Lindgren, Hyperfine Interact. **34**, 217 (1987).

[26] B. Lindgren and A. Ghandour, Hyperfine Interact. **78**, 291 (1993).

[27] A. M. Ghandour and B. Lindgren, in thesis by A. M. Ghandour, Acta Universitatis Upsaliensis, Uppsala 1995, ISBN 91-554-3513-0.

[28] C. R. Laurens, M. F. Rosu, F. Pleiter, and L. Niesen, Phys. Rev. Lett. **78**, 4075 (1997); Hyperfine Interact. **120/121**, 59 (1999).

[29] J. Korecki and U. Gradmann, Phys. Rev. Lett. **55**, 2491 (1985); Europhys. Lett. **2**, 651 (1986).

[30] O. Hjortstam, J. Trygg, J. M. Wills, B. Johansson, and O. Eriksson, Phys. Rev. B **53**, 9204 (1996).

[31] S. Ohnishi, A. J. Freeman, and M. Weinert, Phys. Rev.
     B **28**, 6741 (1983).
[32] G. Filleböck, private communication, Annual report:
     "Jahresbericht Festkörper- und Clusterphysik", Uni-
     versität Konstanz, 1997.
[33] R. Wesche, R. Fink, T. Klas, G. Krausch, R. Platzer,
     J. Voigt, and G. Schatz, J. Phys. Condens. Matter **1**,
     7407 (1989).
[34] B. Lindgren, Hyperfine Interact. (C) **1**, 613 (1996).

[35] K. Potzer, H. H. Bertschat, A. Burchard, D. Forkel-
     Wirth, H. Granzer, H. Niehus, S. Seeger, and W.-D.
     Zeitz, Nucl. Instrum. Methods Phys. Res. B **146**, 618
     (1998).
[36] D. H. Rosenblatt, S. D. Kevan, J. G. Tobin, R. F. Davis,
     M. G. Mason, D. R. Denley, D. A. Shirley, Y. Huang,
     and S. Y. Tong, Phys. Rev. **B26**, 1812 (1982), D. H.
     Rosenblatt, S. D. Kevan, J. G. Tobin, R. F. Davis,
     M. G. Mason, D. A. Shirley, J. C. Tang, and S. Y.
     Tong, Phys. Rev. **B26**, 3181 (1982).